Journal of Environmental Chemical Engineering 12 (2024) 113497

Contents lists available at ScienceDirect

Journal of Environmental Chemical Engineering

journal homepage: www.elsevier.com/locate/jece

From agricultural wastes to advanced materials for environmental applications: Rice husk-derived adsorbents for heavy metals removal from wastewater

Valentina Gargiulo [a,*], Francesco Di Natale [b], Michela Alfe [a]

[a] Institute of Sciences and Technologies for Sustainable Energy and Mobility-CNR-STEMS, Via Guglielmo Marconi 4, Naples 80125, Italy
[b] Dipartimento di Ingegneria Chimica, dei Materiali e della Produzione Industriale, University of Naples Federico II, P.le V. Tecchio 80, Naples 80125, Italy

ARTICLE INFO

Keywords:
Carbonized rice husk
Composite materials
Iron oxide
Heavy metals adsorption
Wastewater treatment

ABSTRACT

Agroindustry annually generates enormous amounts of residues, and their re-utilization is a convenient approach to mitigate environmental pollution and increase energy savings. Rice husk (RH) is one of the most widely available agricultural wastes in many countries of the world. RH and its ashes are often used directly for manufacturing and synthesizing new materials with added-value features. In this work, the preparation of composite materials for wastewater treatment has been explored by producing and testing mesoporous iron-oxide/RH composites for heavy metal adsorption. The composites were fully characterized and their application to the removal of Pb^{2+} and Cu^{2+} ions from model aqueous solutions at different pH values was tested to evaluate their adsorption performances and select those materials more suited for realistic applications. Our results indicated that the composite materials exhibited higher metal adsorption capacities than the pristine carbonized RH and the iron components, highlighting a synergism between the carbonized RH and iron-oxide phases.

1. Introduction

Many industries, such as metal plating, mining, tanneries, painting, and car manufacturing, as well as agricultural activities dealing with the use of fertilizer and fungicidal compounds, are among the main ones responsible for heavy-metal contamination of aqueous waste streams [1,2]. Heavy metals are not biodegradable and because of their high solubility in aquatic environments tend to accumulate in living organisms, causing various diseases and disorders [2,3]. To reduce heavy metal pollution, different treatment processes for decontaminating waste streams, have been developed. The main treatment processes for heavy metal removal from wastewaters include lime precipitation, coagulation, foam flotation, filtration, use of membrane, ion exchange, aerobic and anaerobic treatments, oxidation processes, solvent extraction, adsorption, electrolysis, microbial reduction, and activated sludge [2]. Unfortunately, most of these methods require a not negligible financial input and their use is restricted because of cost factors overriding the importance of pollution control [4,5]. Besides, many of these methods are very effective under steady pollutant concentrations, a property that is rarely achieved with real wastewater.

Among the different available wastewater treatment technologies, the process based on the use of solid sorbents is considered the best choice because of its low execution costs, ease of operation, simplicity of design, and fast adaptation to variable pollutant concentrations [4,5]. In addition, the adsorption process can remove/minimize different types of pollutants and thus it has a wide applicability in water pollution control.

Given these potentialities, several commercial materials have been extensively investigated as adsorbents in water pollution control. The most studied ones include silica gel, activated alumina, zeolites, and activated carbons. State-of-the-art research is focused on the design of adsorbents matching performances and competitive costs for effective water pollution control. In the end, safe disposal of pollutants-laden adsorbents is another important topic of concern that should not be overlooked [6].

The interest in carbon-rich adsorbents derived from agricultural and household biomass residues for the sequestration of different types of pollutants (dyes, heavy metals, and crude oil components) has constantly increased [7,8]. These adsorbents exhibited numerous advantages over non-carbonaceous materials: they are chemically and thermally stable, they are characterized by very high pore volumes and

* Corresponding author.
E-mail address: valentina.gargiulo@stems.cnr.it (V. Gargiulo).

https://doi.org/10.1016/j.jece.2024.113497
Received 17 March 2024; Received in revised form 17 June 2024; Accepted 2 July 2024
Available online 13 July 2024

Table 1
Materials composition. C and H weight percentage contents have been measured by ultimate analysis; ashes have been determined by TG after combustion in pure oxygen at 800°C (the maximum relative error observed was ±0.75 % of the average values).

	C (wt%)	H (wt%)	Ashes (wt%)	Others* (wt%)
cRH	42.3	1.5	47.6	8.6
FM	<0.03	<0.07	>99.9	-
cRH_w	44.5	1.06	42.47	11.97
cRH_{NaOH}	78.8	1.09	7.11	13.00
cRH-FM	43.7	0.43	52.16	3.71
cRH_{NaOH}-FM	73.7	1.11	16.9	8.29

* Evaluated by difference and including nitrogen, oxygen, and non-metals elements

Table 2
Textural characteristics.

Sample	BET area m^2/g	V_t (p/p^0=0.99) cm^3/g	V_μ 10^{-2} cm^3/g
cRH	162	0.102	2.46
cRHw	107	0.077	2.49
cRH_{NaOH}	335	0.370	10.1
cRH-FM	199	0.232	4.89
cRH_{NaOH}-FM	371	0.360	13.7
FM	136	0.327	3.11

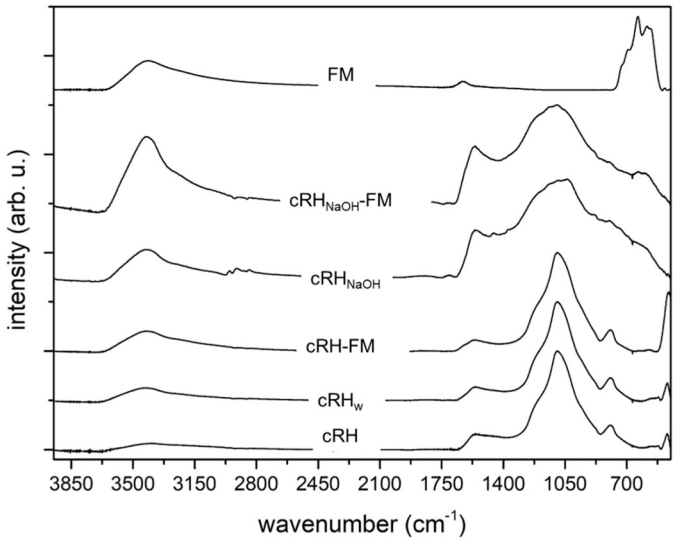

Fig. 1. FTIR spectra of the materials acquired on KBr pellets in the 500–3900 cm^{-1} range.

specific surface areas, they show high adsorption capacity and outstanding cycling performances, they can be easily produced by a combined pyrolysis/activation process and they can be regenerated easily [7,8]. Moreover, their native hydrophobic nature leads to their adsorption efficiency in the gas phase not being affected by the presence of moisture. Finally, the carbonaceous adsorbent surface is prone to be modified through the incorporation of different functional groups [9].

In general, an adsorbent can be termed as a low-cost adsorbent if it requires little processing and itis either abundant in nature, or it is a non-hazardous by-product or waste material from another industry. Of course, improved sorption capacity may compensate for the cost of additional processing. Low-cost adsorbents can be prepared by utilizing abundant and inexpensive raw materials that are characterized by high organic (carbon) and low inorganic contents and are easily activated. Sorbents derived from recycling and/or re-use of wastes used as starting

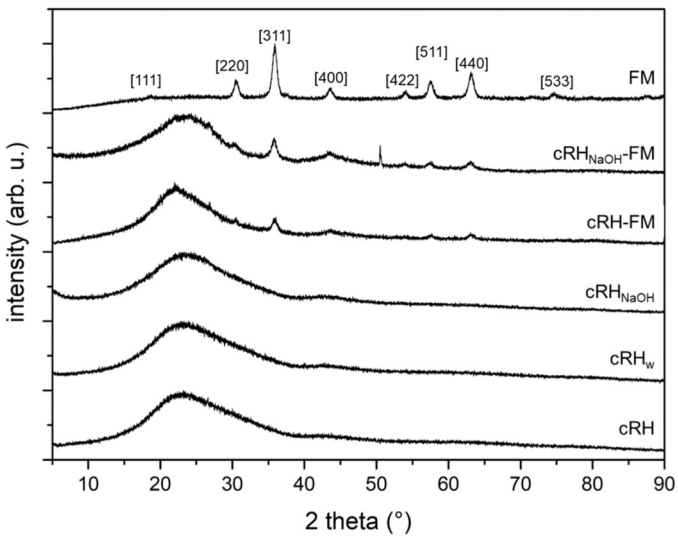

Fig. 2. XRD patterns of the materials.

valued material as alternatives for their disposal are particularly welcome. Agricultural solid wastes embody most of these features and they are very common in every country, and they represent very cheap resources that can be converted into new materials with excellent properties. Agroindustry annually generates enormous amounts of residues (around five billion metric tons in 2020–2021 [10]) and their reduction by utilization might mitigate environmental pollution and increase energy savings. The preparation of low-cost adsorbents from waste materials could be an option to reduce agro-industrial wastes dumping with possible economic and environmental advantages. Anyway, the use of lignocellulosic biomass has some drawbacks (for example physical instability of lignin component and low sorption capacity), and, it is therefore necessary to perform suitable chemical or physical treatments for removing metallic impurities and stabilizing lignin and the other components [7,8]. Examples of raw agricultural wastes successfully used for the preparation of carbon-rich adsorbents include coconut shells, cotton stalks, sugarcane bagasse, coir pith, straw, rice husk, sawdust, coconut husk, oil palm shell, neem bark, peanuts, olive wastes, almond shells, apricots and cherries stones and wastes resulting from the production of cereals [4,6–8,10–13].

Rice husk (RH) is one of the most widely available agricultural wastes around the world. Annually, 571 million tons of rice are produced, and 140 million tons of RH waste are generated [14]. RH finds application basically as a heating source or as a provider of nutrients in the soil, but many times it is simply dumped into the environment [15]. RH, so, could represent a renewable and sustainable carbon resource, and for this reason, it has been investigated for the synthesis of advanced materials for various applications [16–18].

RH is a lignocellulose biomass containing 28–30 % inorganic and 70–72 % organic components. The mineral components of RH are mostly composed of silica (87–97 wt% of total ashes) and calcium- and potassium-based compounds. The RH composition depends on several factors including geological location, rice variety, climate variation, cultivation methods, and fertilizers used in the paddy growth [14,15].

RH as well as RH ashes (RHA) have been intensively investigated as an adsorbent for the removal of heavy metals from wastewater. It was reported that materials obtained by modifying RH present a better adsorption capacity for the removal of heavy metals than native RH. Various approaches were adopted for the modification of RH, including combined pyrolysis/activation processes and surface modification [17,19]. Among them, one of the most common activation/functionalization methods involves the oxidation of surface functional groups with nitric acid, which is used to promote the formation of carboxylic acids. Rice

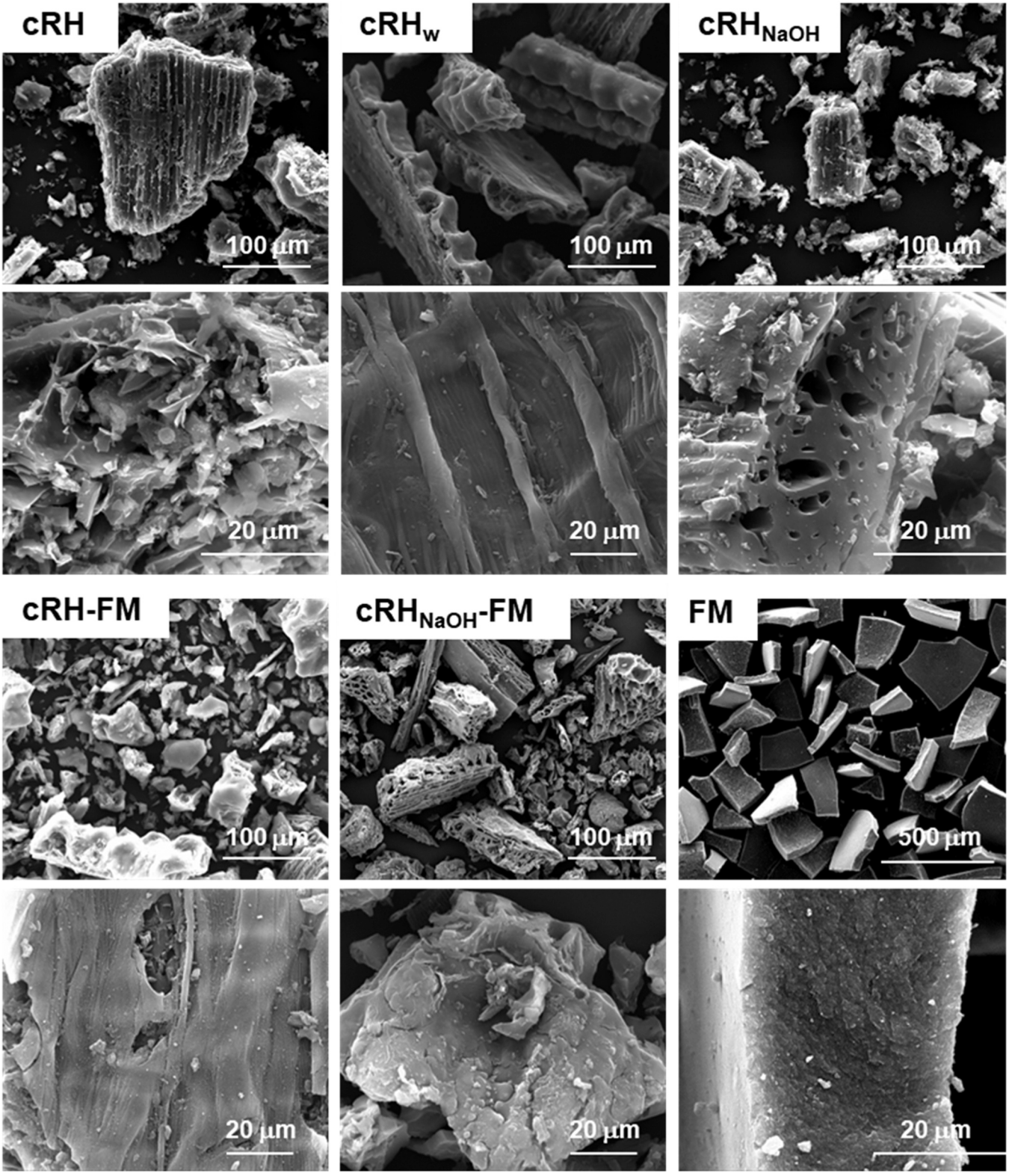

Fig. 3. SEM images of the materials at different magnifications.

husks functionalized with nitric acids act as reversible ion exchangers.

Some authors also proposed the production of iron-oxide/RH hybrid materials with improved adsorption properties compared to native RH [20–27]. Porous carbon-containing iron oxides have received increasing consideration due to their application in a broad range of fields including catalysts for catalytic wet peroxide oxidation, adsorbents for removal of heavy metal ions/organic pollutants from wastewater, electromagnetic microwave absorbers, gas sorption (mainly CO_2) and catalyst for anaerobic digestion by enhancing the electron transfer efficiency [28]. Iron-oxide/RH hybrid materials have been proposed for different remediation purposes: removal of organic pollutants (dyes, drugs, toxins, hydrocarbons [20–24]) and heavy metals [25,26]. Zhang

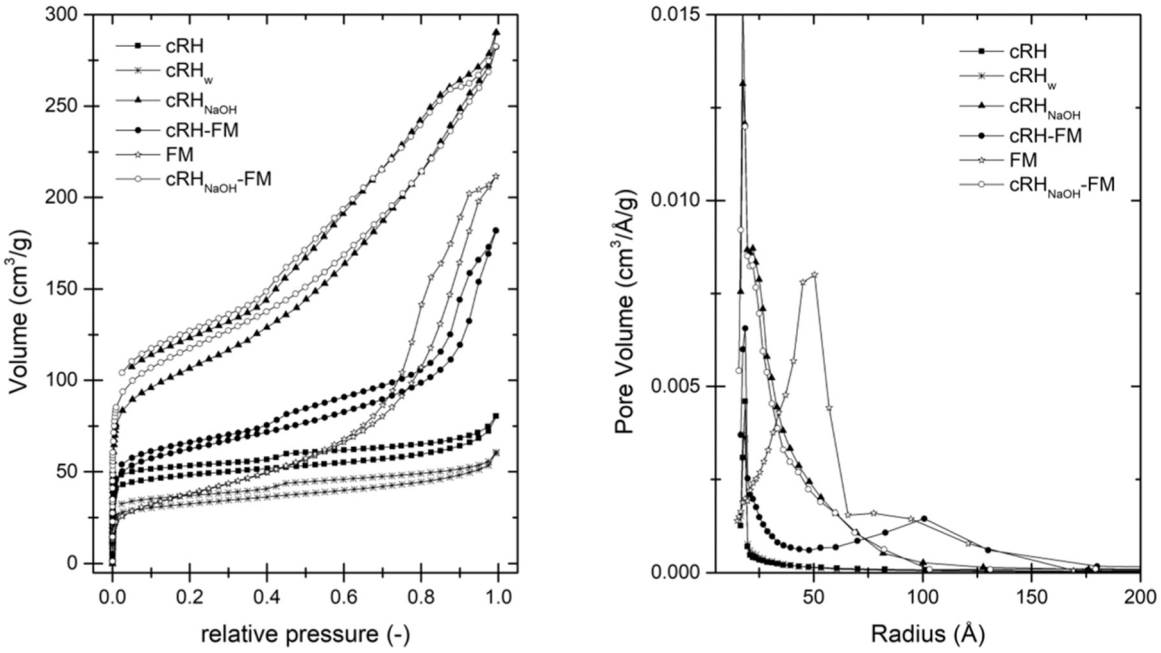

Fig. 4. left panel: Ar adsorption/desorption isotherms of FM, raw cRH, cRH_w, cRH_{NaOH}, cRH-FM, and cRH_{NaOH}-FM at 87 K. right panel: Pore-size distributions (PSD) evaluated by BJH model.

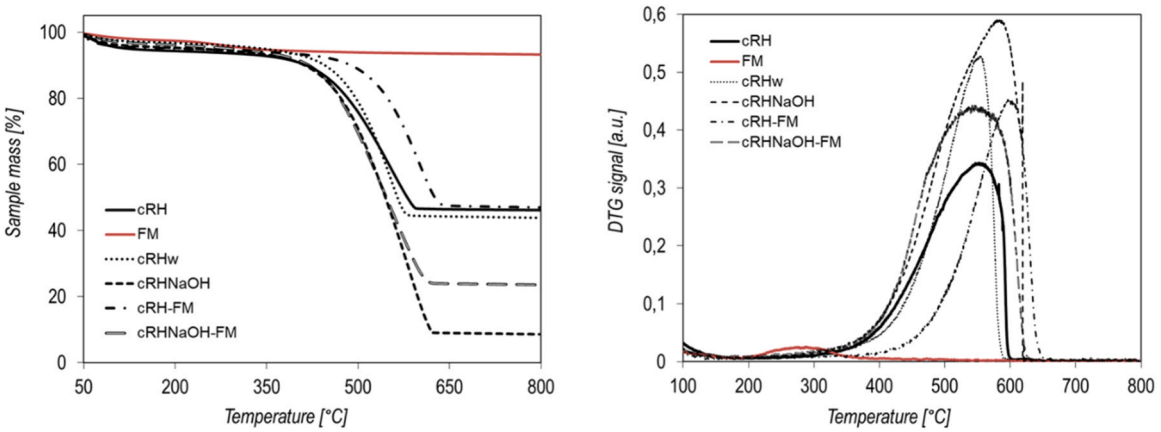

Fig. 5. TG profiles (a) and the corresponding DTG curves (b) of analyses performed under oxidative atmosphere (synthetic air, 40 mL/min) up to 800°C applying a heating rate of 10 °C/min.

et al. [27] demonstrated that porous iron-oxide/RH hybrid materials with a quite high surface area (527 m^2/g) can be produced by exploiting a combined activation and iron loading process [27].

In this framework, to exploit the advantages and shortcomings of using real biomass as a starting material for the preparation of sorbents for heavy metals removal from wastewater, we have prepared a set of iron-oxide/RH composite materials. To this aim, carbonized RH (hereinafter cRH) was coated with iron oxide particles (FM). The influence of the inorganic components of the cRH (mainly SiO_2) was also studied by pre-treating the cRH with distilled water rinsing and alkaline solutions. The exploitation of hybridization with magnetite particles plays a dual role: 1) introducing a functionalization useful to enhance synergistically the sorption performances of carbonized rice husk toward heavy metal ions; 2) facilitating sorbent recovery after use by exploiting the magnetic properties of the hybrid particles attracted by a magnetic field. This fact is of great interest for large-scale adsorption plants, where the separation of adsorbent particles plays a role as significant as their adsorption capacity.

The aim of the work was to introduce the preparation and the characterization of hybrid materials composed of cRH (as it is and treated with NaOH alkaline solutions) bearing a nominal amount of FM up to 10 wt%. A set of explorative adsorption tests was carried out aimed to investigate the best match between the two components of the hybrids (FM and cRH as it is and treated with NaOH alkaline solutions (cRH_w/cRH_{NaOH})) suitable to enhance the adsorption capacity toward heavy metals (copper and lead ions model solutions).

Copper and lead ions have been chosen because of their different characteristics: following Pearson's HSAB theory [29,30], copper ions are harder than lead ions. This means that among them, copper ions have a larger tendency to be adsorbed over oxygenated organics groups, while lead ions prefer soft groups such as chlorides, sulfides, or iodine. Taking into consideration also redox potentials, many studies demonstrated that the main groups that are involved in the adsorption of Cu^{2+} ions are the carboxylic groups, lactones, phenolic, and carbonyl groups [31] while in the case of Pb^{2+} ions removal, only carboxylic groups are involved and not phenolic and carbonyl groups [32]. In the end, the two metal ions are present in a wide number of industrial and civil wastewaters and their removal remains a critical issue for many applications.

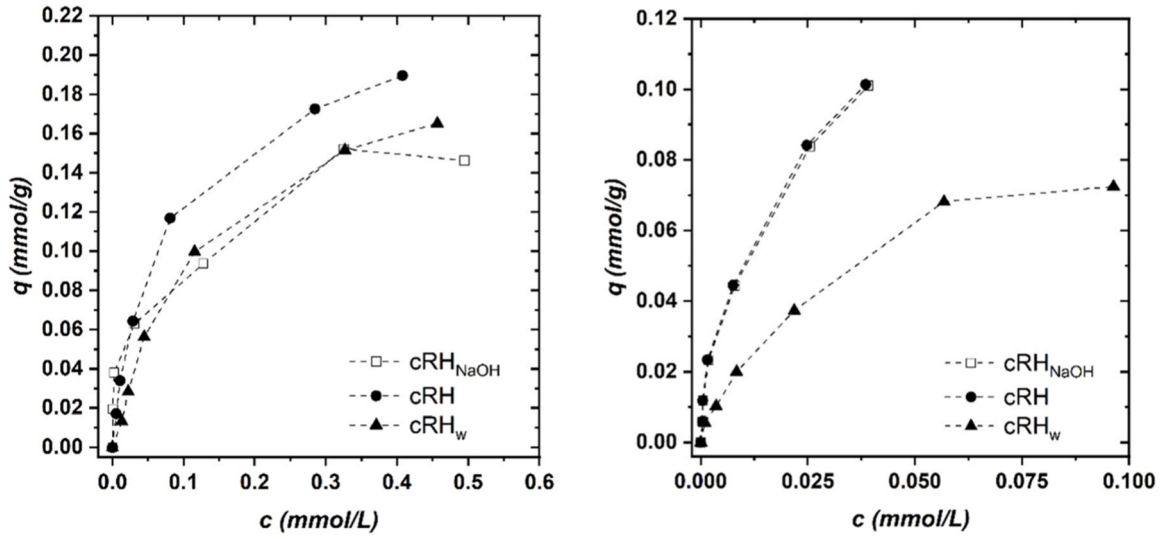

Fig. 6. Copper (left) and lead (right) ions adsorption isotherms of cRH, cRH$_w$, and cRH$_{NaOH}$. (Mass of adsorbent = 20 mg, volume of aqueous model solution = 10 mL, metal ion initial concentration between 0 and 50 mg/L, equilibrium pH between 6 and 7, T = 20°C). The ions concentration is affected by an error lower than 4 % while that of the adsorption capacity is lower than 6 %. Lines are guides for the eyes.

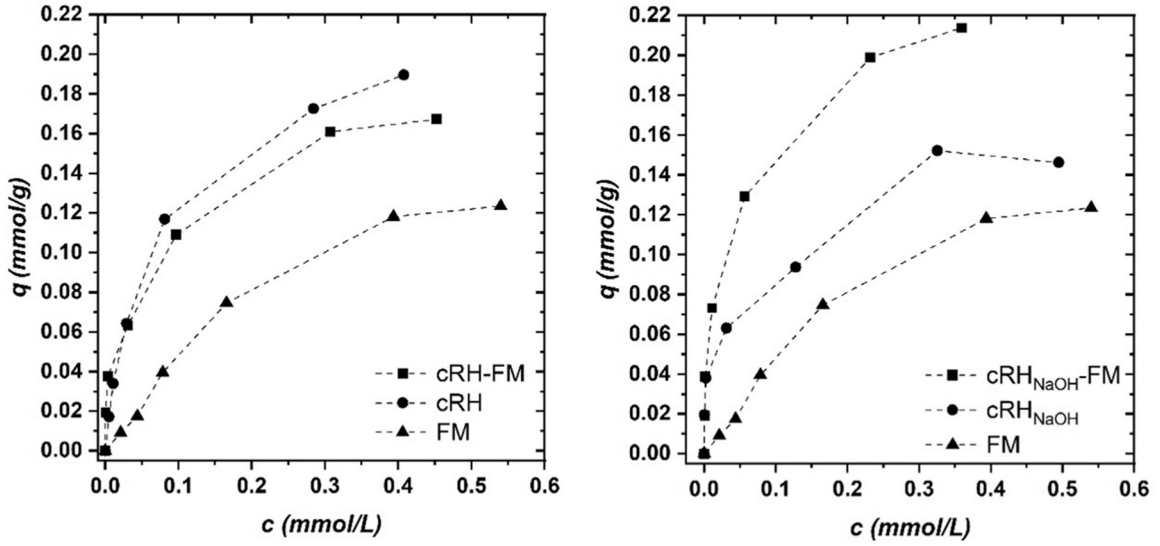

Fig. 7. Copper ions adsorption isotherms of cRH, cRH$_{NaOH}$, cRH-FM, cRH$_{NaOH}$-FM and FM. (Mass of adsorbent = 20 mg, volume of aqueous model solution = 10 mL, metal ion initial concentration between 0 and 50 mg/L (0.787 mmol/L), equilibrium pH between 6 and 7, T = 20°C). The ions concentration is affected by an error lower than 4 % while that of the adsorption capacity is lower than 6 %. Lines are guides for the eyes.

The experiments have been carried out in copper and lead model solutions at standard room temperature, exploring concentrations in a range below 50 mg/L, which is consistent, and even larger, than the typical ranges of concentrations treated by adsorption in real wastewaters. Acidic solutions have been also considered since they often characterize industrial effluents polluted by metals. Preliminary desorption tests have been also carried out on the best-performing materials to verify whether the used rice husk and the composite material adsorption exploit reversible or irreversible adsorption of copper and lead ions.

2. Experimental section

2.1. Materials

All chemicals were purchased from Merck KGaA, Darmstadt, Germany, as analytical grade reagents, and used as received.

RH derived from a deposit in Kazakhstan and details about its composition and its thermal transformation into carbonized rice husk (hereinafter indicated as cRH) are reported elsewhere [33]. cRH was selected as the starting material to produce the adsorbents analyzed in this work. Details about RH and cRH compositions are provided in the supporting material section (Tables S1 and S2)

2.2. Materials synthesis

cRH purification (water-soluble species removal) was performed by treating ground-milled cRH (1 g) with distilled water (50 mL) for 1 h under stirring. The solid (labeled in the following as cRH$_w$) was then recovered by under-vacuum filtration and dried at 100°C.

cRH desilication was performed following the procedure reported in Gargiulo et al., 2018 [33] by treating cRH with a strong alkali aqueous solution. To this aim, 10 g of ground milled cRH were suspended in 140 mL of distilled water and treated with 60 mL of NaOH 5 M for 2 h at 80°C under stirring. The solid (labeled in the following as cRH$_{NaOH}$) was

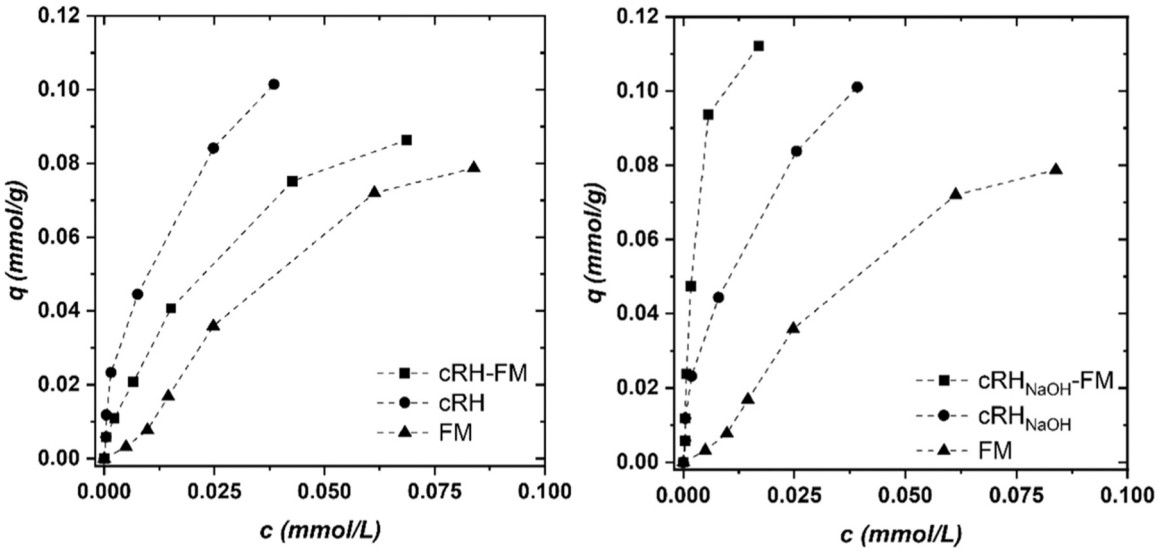

Fig. 8. Lead ions adsorption isotherms of cRH, cRH$_{NaOH}$, cRH-FM, cRH$_{NaOH}$-FM, and FM. (Mass of adsorbent = 20 mg, volume of aqueous model solution = 10 mL, metal ion initial concentration between 0 and 50 mg/L (0.241 mmol/L), equilibrium pH between 6 and 7, T = 20°C). The ions concentration is affected by an error lower than 4 % while that of the adsorption capacity is lower than 6 %. Lines are guides for the eyes.

then recovered by under-vacuum filtration, washed many times with distilled water till neutrality, and then dried at 100°C.

Composite materials containing cRH or cRH$_{NaOH}$ and magnetite (Fe_3O_4, indicated as FM in the following) were produced according to the co-precipitation procedure reported in former works [9,33,34] and briefly described in the following. An amount of cRH or cRH$_{NaOH}$ (3 g) was suspended with 100 mL of distilled water and treated with 0.7 g of $FeCl_3$·6 H_2O and 0.36 g di $FeSO_4$·7 H_2O under stirring for 30 min. After that, the pH was adjusted to 10 by adding 10 mL of ammonium hydroxide solution (28 % NH_3 in H_2O), and the mixture was kept for 1 h at 90 °C under stirring. In the end, each composite (labeled as cRH-FM and cRH$_{NaOH}$-FM, respectively, where FM stands for magnetite) was then recovered by under-vacuum filtration, washed with distilled water till neutrality and then dried at 100°C. FM precursors were added in such an amount to obtain composites containing a theoretical percentage of iron oxide around 10 wt%.

Bare magnetite (FM) was also prepared for comparison according to the procedure reported in [9,33,34]: 1.4 g of $FeCl_3$·6 H_2O and 0.70 g $FeSO_4$·7 H_2O were dissolved in 100 mL of distilled water and the solution was kept at 30 °C for 15 min, after that the pH was adjusted to 10 by the addition of 10 mL of ammonium hydroxide solution (28 % NH_3 in H_2O). The mixture was kept for 1 h at 90 °C under stirring and then cooled to room temperature. The solid was recovered through under-vacuum filtration and washed with water many times to remove all traces of unreacted salts and ammonium hydroxide. The sample was dried at 100°C.

2.3. Material characterization methods

The carbon and hydrogen contents of the samples were determined by ultimate analysis according to the ASTM D3176–15 standard. A LECO 628 analyzer calibrated with ethylenediaminetetraacetic acid (EDTA) was used for the measurements. For each sample, three replicates were performed, and the average values were reported (the maximum relative error was around 0.75 %).

Ash content was evaluated by burning the samples at 800°C under pure O_2 until mass constancy in a TGA 701 LECO analyzer according to the ASTM D7582–15 standard.

Fourier transform infrared (FTIR) spectra were acquired on a Perkin Elmer Frontier MIR spectrometer in transmittance mode. Solid sample dispersions were prepared by mixing and grinding the powdered materials (0.5–1 wt%) with KBr. Pellets (13 mm in diameter) of the solid mixtures were obtained upon compression at 1 bar for 5 minutes. The spectra were recorded in the 450–4000 cm^{-1} wavenumber range by collecting 8 scans and correcting the background noise.

The thermal stability of the samples was evaluated by thermogravimetric analysis (TGA) performed on a Perkin Elmer STA 6000. The samples were heated in an oxidative environment (air) from 50°C up to 800°C at a rate of 10 °C/min. Samples were loaded in an alumina crucible thermally preconditioned up to 950°C for an accurate mass loss evaluation.

BET specific surface area (SA) of the samples was measured by Ar adsorption at 87 K using a Quantachrome Autosorb 1 apparatus. The samples were outgassed under vacuum at 120 °C before the analysis. Adsorption/desorption data were processed following the BET equation to evaluate the specific surface area (SSA) and with the BJH model to evaluate the pore size distribution (PSD) [35,36].

Scanning electron microscopy (SEM) was carried out with an FEI Inspect microscope equipped with an EDS Oxford AZtecLiveLite probe and Xplore 30 detector for elemental analysis. The imaging was performed on powdered samples, previously dried and sputter-coated with a thin layer of gold to avoid charging.

X-ray diffraction (XRD) analyses were carried out on a Rigaku Miniflex 600 diffractometer operating in the 3 – 90 °2θ range with a Cu Kα radiation (λ = 1.54056 Å), a step size of 0.02°, a counting time of 80 s per step and using a low background holder. The signal-to-noise in the patterns of composite materials was improved by eliminating the fluorescence deriving from Fe with the suppression tool provided by the instrument.

2.4. Adsorption tests

The adsorption tests were carried out using single metal model aqueous solutions containing either copper or lead ions in different concentrations. The solutions were contacted with a given mass of sorbent (m (g)) in glass vials with screw caps, gently agitated by an orbital shaker at 50 rpm, and kept at constant temperature in a PID-controlled thermostatic oven. The model copper or lead aqueous solutions were obtained by dissolving the corresponding nitrate salt ($Cu(NO_3)_2$·2.5 H_2O or $Pb(NO_3)_2$) in double-distilled water. The initial solution pH value was adjusted by the addition of NaOH and HNO_3 solutions prepared from commercial reagents. Nitrate salts and HNO_3 as well as NaOH were

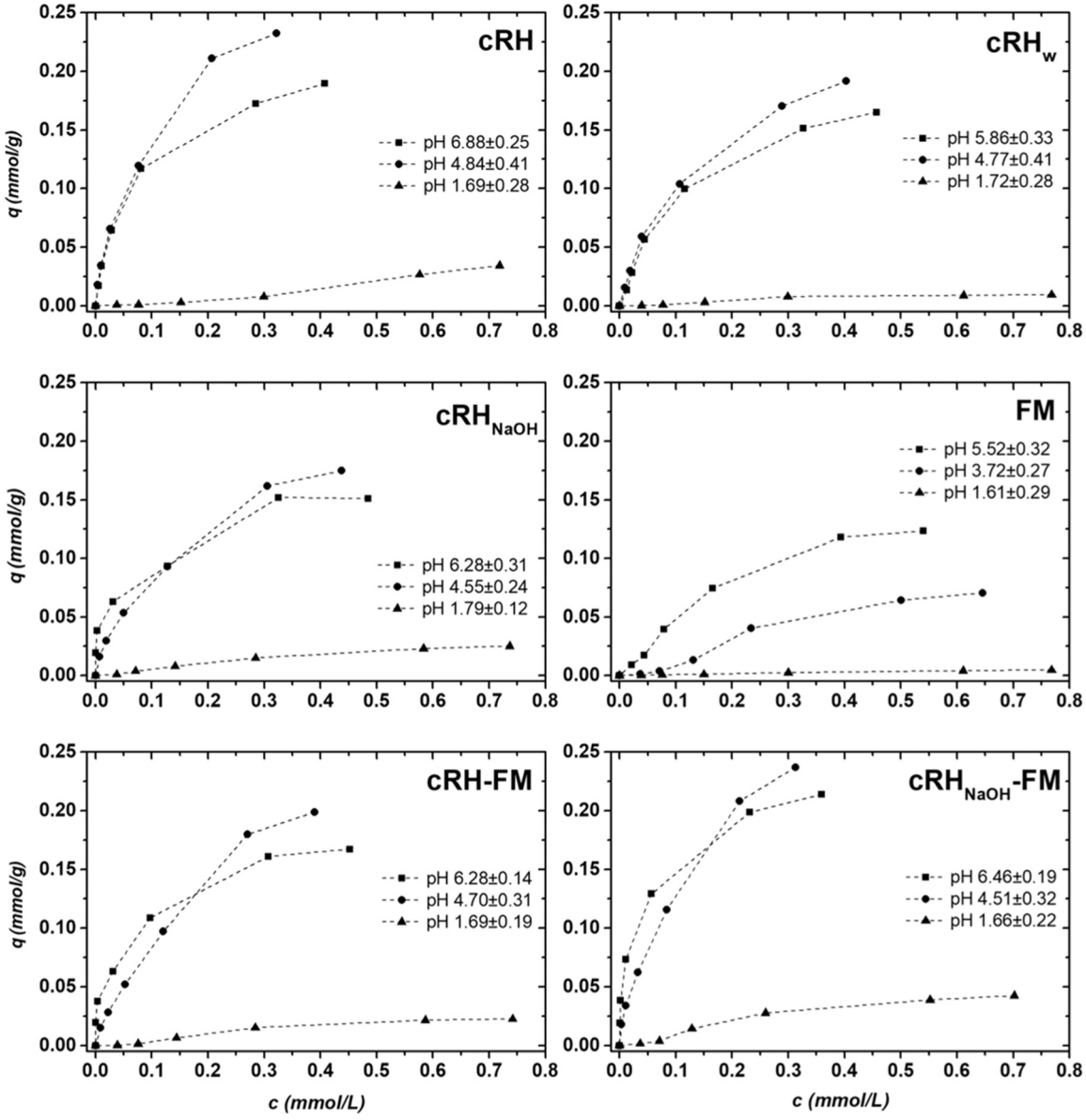

Fig. 9. Copper ions adsorption isotherms of the different adsorbents at different equilibrium pH values. T = 20 °C, adsorbent mass 20 mg, volume 10 mL, metal ion concentration between 0 and 50 mg/L (0.787 mmol/L). The ions concentration is affected by an error lower than 4 % while that of the adsorption capacity is lower than 6 %. Lines are guides for the eyes.

purposely chosen to minimize the interferences with heavy metal ions adsorption and because they are a standard choice in adsorption tests reported in the literature. Indeed, the formation of nitrate salts of Cu(II) and Pb(II) is by far negligible compared with other ions, limiting the ion speciation to Cu^{2+}, $Pb^{2+,}$ and their hydroxide ions (e.g. $CuOH^{+}$, $PbOH^{+}$, $Cu(OH)_2$, $Pb(OH)_2$, $Cu(OH)_3^-$, $Pb(OH)_3^-$, etc) [29]. The pH was not further modified during the tests.

Isotherm studies were performed by using 20 mg of adsorbent in 10 mL of aqueous model solution and by varying the metal ion initial concentration from 0 to 50 mg/L. To evaluate the effect of pH on the adsorption capacities of the tested materials, tests at pH 2, 4 and 6 were performed. Preliminary tests showed that 72 h and 120 h were enough to reach the equilibrium conditions in the experimental tests for lead and copper ion adsorptions, respectively. When equilibrium conditions were achieved, the total metal ion concentration in the solution was measured by atomic absorption spectrophotometry (AAS-F) by using a Varian SpectrAA-220 following the standard methods IRSA CNR 3250 and 3230 for copper and lead ions, respectively. The pH values of each solution at the beginning and the end of the tests were measured by a Thermo Scientific Orion Star A111 pHmeter.

Experimental data were expressed as correlations between the equilibrium total metal concentration, c (mmol/L), and the metal adsorption capacity, q (mmol/g), at given temperature and equilibrium pH values. To allow an easier comparison of data for copper and lead ions adsorption, the concentrations are expressed in mol/L and mmol/g in place of the most common mg/L and mg/g.

The adsorbent performances were calculated as reported previously [37] and for the sake of completeness, additional details are reported in the supporting information section (Section S1).

All tests were performed in triplicate and average values are reported. The accuracy of analytical techniques was checked by the evaluation of the relative standard deviation (RSD) of each sample analysis. Typical values of the RSD for the heavy metals concentration in solution are below 1 %. Among the replicates, the average values of c are affected by an error lower than 4 %. The values of q are affected by an error lower than 6 %.

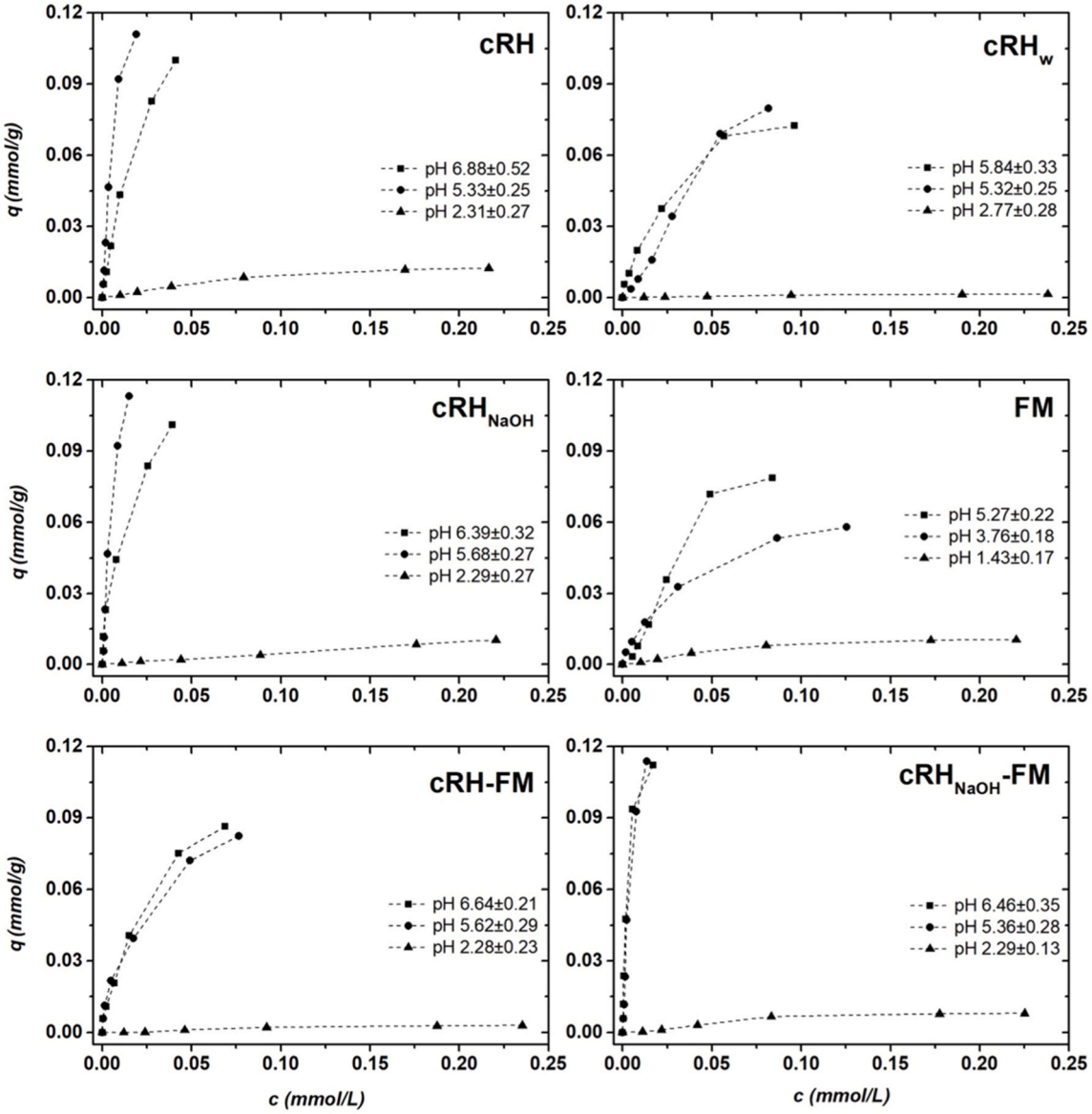

Fig. 10. Lead adsorption isotherms of the different adsorbents at different pH values. T = 20 °C, adsorbent mass 20 mg, volume 10 mL, metal ion concentration between 0 and 50 mg/L (0.241 mmol/L). The ions concentration is affected by an error lower than 4 % while that of the adsorption capacity is lower than 6 %. Lines are guides for the eyes.

The adsorption isotherms have been preliminary modeled following a multicomponent Langmuir model [38–41], to account for the possible competition between the target metals ions and the H_3O^+, c_H, in mmol/L and to account for the effects of solution pH on the adsorption process. The model equation is:

$$q = \frac{q\max \bullet K \bullet c}{1 + K \bullet c + K_H \bullet c\mathrm{H}} \quad (1)$$

Where q_{max} is the maximum adsorption capacity in mmol/g, K and K_H are, respectively, the Langmuir equilibrium constants for the metal ion and the H_3O^+, in mM^{-1}, which are assumed to be well approximated as a function of the temperature and of the Gibbs' free energy of adsorption at standard conditions ΔG°, neglecting temperature effects on the Gibbs' free energy:

$$q = \frac{q\max \bullet \exp[-\Delta G^\circ/RT] \bullet c/c_{ref}}{1 + \exp[-\Delta G^\circ/RT] \bullet c/c_{ref} + \exp[-\Delta G_H{}^\circ/RT] \bullet c\mathrm{H}/c_{ref}} \quad (2)$$

In this formulation, c_{ref} is 1 M and is needed to adapt the units of measures Eq.(2). If the sorbents act as pure ionic exchangers with one single surface group, their behavior can be well described by simple ion complexation models [29,30], but if, as it happens for adsorption with biomasses or carbon-based materials, multiple adsorption sites are present, the Langmuir model can be better used to describe the competition between H_3O^+ and Cu^{2+}/Pb^{2+} considering all the functional groups as represented by one family of "average" functional groups having adsorption energy represented by a Gaussian distribution function characterized by a mean and a standard deviation value. The maximum amount of the average adsorption sites is given by the value of q_{max}.

Several other models have been proposed in the pertinent literature to describe multicomponent adsorption processes [42–44], but these models require a much larger number of fitting parameters (at least five) and are thought to analyze simultaneous adsorption of different ions, rather than describe interactions between ions and H_3O^+.

To preliminary compare the performances of the sorbents toward copper and lead ions, the partition coefficient, H, of the adsorption isotherms has been calculated too. This is the ratio between the

Table 3
Parameters evaluated by applying the additive-competitive Langmuir model (Eq.1).

Copper ions adsorption						
	$q_{max,}$[mmol/g]	$\Delta G^{\circ}, J/mol$		$\Delta G^{\circ}_{H}, J/mol$		R^2
		Average	Standard dev.	Average	Standard dev.	
cRH	0.25±0.02	-23507	9712	-19856	8710	0.9716
cRH_w	0.23±0.01	-22092	8696	-20605	9288	0.9848
cRH_{NaOH}	0.21±0.02	-22447	9546	-19296	8617	0.9587
cRH-FM	0.24±0.02	-22163	9345	-19184	8692	0.9613
cRH_{NaOH}-FM	0.27±0.02	-23650	10022	-18994	8217	0.9636
FM	0.20±0.02	-20024	7855	-23799	9379	0.9884
Lead ions adsorption						
	$q_{max,}$[mmol/g]	-28555	13182	-24914	11918	R^2
cRH	0.13±0.02	-24297	10764	-27408	13222	0.8697
cRH_w	0.14±0.02	-29927	13631	-27042	13141	0.9668
cRH_{NaOH}	0.12±0.01	-26123	10490	-27680	12986	0.9111
cRH-FM	0.18±0.01	-31027	13255	-29202	13076	0.9982
cRH_{NaOH}-FM	0.15±0.01	-23764	10782	-21832	9486	0.9834
FM	0.14±0.03	-28555	13182	-24914	11918	0.9368

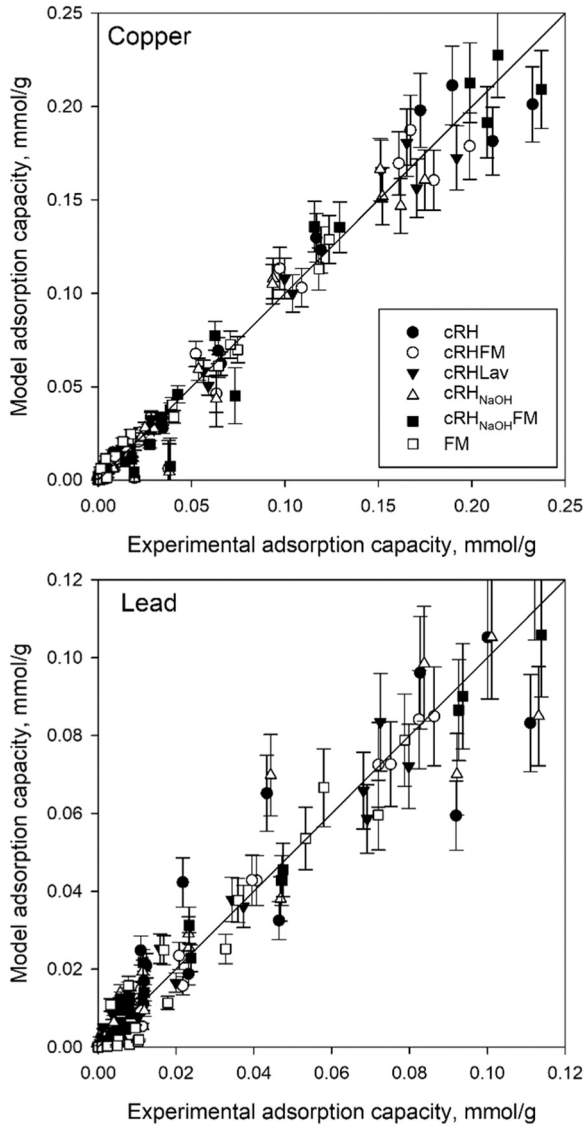

Fig. 11. Parity plots on adsorption capacity for Cu^{2+} and Pb^{2+} ions adsorption data.

adsorption capacity and the solute concentration, q/c. Apart from linear isotherms, this ratio is a function of the solute concentration. To this end, in this work, we will consider the average partition factor at low concentration values, where a linear shape of the adsorption isotherm is likely to be observed. This low-concentration area is important because it covers the typical concentrations where water regulations limits are located. For example, the Italian Environmental Regulations for sewage discharge (D.Lgs. 152/06 Annex 5, Table 3) allows 0.3 mg/L for lead and 0.4 mg/L for copper. Equilibrium adsorption capacity at these concentrations is the most relevant for the design of adsorbers since it determines the minimum dosage of sorbent (kg/m^3) to be used for wastewater depuration. At such low concentrations, it is also likely that competition between ions is limited so the partition coefficient also represents a preliminary estimation of the sorbent selectivity toward lead and copper.

Finally, preliminary desorption tests have been carried out on the bare rice husk sorbent and the best-performing sorbent, for both copper and lead. The tests have been performed at ambient temperature by treating the sorbent with 1 M nitric acid and performing three subsequent adsorption-desorption cycles to exploit potential sorbent reversibility.

3. Results and discussion

3.1. Composition and structural features of materials

Table 1 reports the compositions of the different materials as weight percentage contents of C, H, and other elements including N, O, and other non-metal species ("Others"). The compositions of bare cRH and FM are also reported.

The RH is a biomass very rich in inorganic matter and its percentage becomes more abundant after the carbonization process, passing from 22 wt% to 46 wt% [33]. After the treatment in alkaline conditions, the inorganic phase (mainly composed of SiO_2 and AAEMs' oxides) in cRH_{NaOH} is significantly reduced compared with those of cRH and cRH_w. The presence of FM in the two composite materials leads to a percentage reduction of the carbon content and a corresponding increase in the content of ashes (Table 1). Such a slight increase is consistent with the introduction of FM.

Insights about the effect of the strong alkaline treatment on cRH features and composition were highlighted also by FTIR analysis. FTIR spectra acquired in transmission mode are shown in Fig. 1. Peaks ascribable to SiO_2 (Si-O-Si and Si-O stretching vibrations) at ~1100 cm^{-1} and ~800 cm^{-1} typically observed in RH-derived carbons are detected in the spectra of cRH, cRH_w and cRH-FM, while broad overlapping bands between 600 and 1700 cm^{-1}, ascribable to an amorphous carbon

Table 4
Theoretical maximum q_{max} (mg/g) of rice husk-derived carbons reported by recent literature.

Pb^{2+}						
Adsorbent	**Preparation**	**BET Surface area (m^2/g)**	**pH_{pzc}**	**%C**	**q_{max} Langmuir (mg/g)**	**ref**
Rice husk-derived activated carbon (RHAC)	NaOH activation and carbonization (400°C, N_2, 2 h)	253.4	-	44	1666.67	[53]
Unactivated rice husk carbon (URHC)	pyrolysis (350°C)	-	-	-	8.56	[54]
Activated rice husk carbon (ARHC)	ammonium chloride pre-treatment and pyrolysis (350°C)	-	-	-	12.99	[54]
Rice husk ash	carbonization (300°C)	0.632	7.1	53.1	14.1	[55]
Rice husk ash	carbonization (500°C)	45.27	9.5	55.6	21.7	[55]
Rice husk ash	carbonization (700°C)	193.2	9.8	57.1	26.7	[55]
Rice husk ash	burning	57.5	8.5		91.74	[56]
Rice husk biochar	pyrolysis (700°C, N_2)	440	8.4		77.09	[57]
Rice husk biochar	calcination (350°C, O_2-limited environment, 4 h)	27.8	8.01	38.6	29.01	[58]
Rice Husk Activated Carbon	H_3PO_4 activation and carbonization (450°C)	-	-	-	0.1487	[59]
Rice husk biochar	pyrolysis (500°C, N_2) and KOH activation	645.8		36.89	0.11	[60]
Rice husk biochar	pyrolysis (600°C, N_2) and KOH activation	635.8	-	42.84	0.11	[60]
Rice husk biochar	pyrolysis (700°C, N_2) and KOH activation	919.8	-	39.8	0.11	[60]
Rice husk biochar	Pyrolysis (500°C, O_2-limited environment)	-	7.03	-	0.223	[61]
Rice husk biochar	pyrolysis (600°C, N_2)	34.39	-	-	156.250	[62]
Rice husk biochar	pyrolysis (350–450°C)	-	8.10	-	14.20	[63]
Rice husk hydrochar	HTC method (260°C)	21.92	7.23	50.63	5.91	[64]
Rice husk biochar	pyrolysis (500°C, N_2)	4.63	9.07	50.51	6.58	[64]
Magnetic rice husk biochar	$Fe(NO_3)_3$ mixing and pyrolysis (600°C, N_2)	275	6.78	37.6	17.2	[26]
$KMnO_4$-treated rice husk biochar	$KMnO_4$ treatment of magnetic biochar and pyrolysis (600°C, N_2)	137	8.51	21.8	168.7	[26]
Rice husk biochar (cRH)	Carbonization	162	6.88	42.3	27.1	This work
Water-washed rice husk biochar (cRH_w)	Carbonization and H_2O washings	107	5.84	44.5	24.6	This work
Desilicated rice husk biochar (cRH_{NaOH})	Carbonization and NaOH treatment	335	6.39	78.8	26.1	This work
cRH-FM	Carbonization and FM coating	199	6.64	43.7	25.7	This work
cRH_{NaOH}-FM	Carbonization, NaOH treatment, and FM coating	371	6.46	73.7	31.7	This work
Cu^{2+}						
Adsorbent	**Synthesis procedure**	**BET Surface area (m^2/g)**	**pH_{zc}**	**%C**	**q_{max} Langmuir (mg/g)**	**ref**
Rice husk-derived activated carbon (RHAC)	pyrolysis (700°C, N_2) and steam activation	244.3	-	37.29	21.01	[52]
Rice husk ash	Acid activation and calcination (600°C, 1 h)	-	-	49.81	4.127	[48]
Rice husk biochar	calcination (350°C, O_2-limited environment, 4 h)	27.8	8.02	38.6	4.16	[58]
Rice husk biochar	pyrolysis (700°C, N_2)	440	8.4	-	10.60	[57]
Rice Husk Activated Carbon	H_3PO_4 activation and carbonization (450°C)	-	-	-	0.8308	[59]
Rice husk biochar	Pyrolysis (500°C, O_2-limited environment)	-	7.03	-	28.62	[61]
Rice husk biochar	pyrolysis (350–450°C)	-	8.10	-	10.27	[63]
Rice husk biochar	hydrothermal carbonization (200°C, 1.7 MPa)	10.42	5.2	45.25	13.12	[65]
N-doped Rice husk biochar	hydrothermal co-carbonization (200°C, 1.7 MPa) in the presence of *Chlorella pyrenoidosa*	8.13	5.6	49.03	29.11	[65]
Rice husk biochar (cRH)	Carbonization	162	6.88	42.3	16.6	This work
Water-washed rice husk biochar (cRH_w)	Carbonization and H2O washings	107	5.84	44.5	14.9	This work
Desilicated rice husk biochar (cRH_{NaOH})	Carbonization and NaOH treatment	335	6.39	78.8	16.3	This work
cRH-FM	Carbonization and FM coating	199	6.64	43.7	15.4	This work
cRHNaOH-FM	Carbonization, NaOH treatment, and FM coating	371	6.46	73.7	17.3	This work

network, are detected in the spectra of cRH_{NaOH} and cRH_{NaOH}-FM [33]. Stretching signals of Fe-O bonds located below 800 cm^{-1} [9] characterize the FM spectrum and are hardly detected in the spectra of cRH-FM and cRH_{NaOH}-FM as a consequence of the low FM content introduced and the predominance of the carbonaceous background.

To confirm the presence of the desired iron oxide phase (magnetite, Fe_3O_4) in the composite materials, XRD patterns were acquired. The results of the diffractometric survey are reported in Fig. 2, where the XRD patterns have been reported as height normalized plots and shifted on the *y*-axis for clarity. In the XRD patterns of cRH, cRH_w, and cRH_{NaOH}, broad bands typical of silica and amorphous carbon-rich materials are detected [37]. The XRD pattern of FM is also reported for comparison and is consistent with the magnetite pattern [45]. The magnetite signature is also detected in the XRD patterns of cRH-FM and cRH_{NaOH}-FM confirming that the synthetic approach allows for the production of magnetite also in the presence of cRH or cRH_{NaOH} when used as carbonaceous support. This result is further corroborated by the magnetic activity detected in each sample by simply locating a permanent magnet close to each material.

The morphology of the samples was investigated by SEM imaging. In Fig. 3 a collection of images at different magnifications is reported. The images show that the morphology of the starting material (cRH) is mainly preserved through the performed chemical treatments (washing, desilication, and hybridization with FM), while the presence of a

Table 5
Copper and lead partition factors H, in m^3/kg, at low ions concentration for the pH values and sorbent formulations.

Copper ions	pH range		
	5.5–7.0	3.5–5.0	1.0–2.0
cRH	3223.5	4044.2	16.6
cRH_w	1188.4	1603.1	11.6
cRH_{NaOH}	29558.8	1862.5	46.4
cRH-FM	21736.5	1469.9	31.8
cRH_{NaOH}-FM	23977.6	4148.7	69.6
FM	447.0	90.3	7.2
Lead ions	pH range		
	5.5–7.0	3.5–5.0	1.0–2.0
cRH	5393.6	11218.7	112.8
cRH_w	4316.3	879.9	9.2
cRH_{NaOH}	294.2	66.6	0.3
cRH-FM	9972.1	9916.5	13.3
cRH_{NaOH}-FM	474.3	238.6	0.3
FM	1.4	9.8	0.4

wrinkled surface with holes and cavities is suggested by micrographs of cRH_{NaOH}. Bare FM exhibited a very smooth surface, and the surface of cRH-FM and cRH_{NaOH}-FM appears slightly smoother compared with that of the parent materials (cRH and cRH_{NaOH}, respectively) suggesting a homogenous coverage by the FM phase.

The EDX analysis performed on cRH-FM and cRH_{NaOH}-FM confirms the presence of FM in the composites. The iron content was 10 wt% and 6 wt% for cRH-FM and cRH_{NaOH}-FM, respectively. The quite uniform distribution of iron in the structure of both composite materials is also confirmed by the EDX maps (data not shown).

The textural properties of the materials were investigated by Ar adsorption/desorption tests at 87 K. The isotherms of materials are reported in the left panel of Fig. 4, while in the right panel of Fig. 4 the corresponding pore size distributions (PSDs) are shown. The isotherms and PSDs of pure FM and raw cRH are also reported for comparison.

The shape of the isotherms mirrors the different porosity of the samples. In most cases, the shape of the isotherms resembles those typical of mesoporous materials [35]. In the case of FM, a marked hysteresis loop and a consistent gas uptake at relative pressures above 0.5 are detected suggesting the presence of an enhanced mesoporosity [36]. The high gas uptake at very low relative pressures detected for cRH_{NaOH} and cRH_{NaOH}-FM indicated the presence of a microporosity along a very developed mesoporosity.

The adsorption data have been worked out to calculate: 1) the specific surface area values through the BET equation (Table 2); 2) the total pore volume at p/p_0 V_t=0.99 (Table 2) the pore size distribution through the BJH model (Fig. 4, right panel).

BET surface area values above 300 m^2/g have been measured only for the desilicated samples (cRH_{NaOH} and cRH_{NaOH}-FM) suggesting that the inorganic component of cRH (mainly silica) causes pores clogging. This aspect is also supported by the difference between the total pore volume of cRH and those of cRH_{NaOH} and cRH_{NaOH}-FM. Instead, the washing of cRH with water induces a detrimental change in its textural properties, as both the SSA and total pore volume decrease. Conversely, when cRH is covered by FM particles, an increase in the surface area, accompanied by a large increase in mesopores volume, is observed (a feature ascribable to the FM coating). An increase in the surface area is also detected in the case of cRH_{NaOH}-FM, but the increase in pore volumes is attributable to an increase of both mesopores and micropores volumes compared with the bare carbonaceous support (cRH_{NaOH}).

As concerns the pore-size distributions (Fig. 4, right panel), cRH and cRHw exhibited very similar distributions and the same was found for cRH_{NaOH} and cRH_{NaOH}-FM. The presence of a contribution ascribable to the inorganic part (FM) is evidenced by the broad peak centered around 100 Å exhibited by the PSD of cRH-FM (Fig. 4, right panel), whereas the cRH_{NaOH}-FM PSD is dominated by micropores having a size smaller than 50 Å.

The thermal stability of the samples under air was evaluated by TGA. The TG profiles and the corresponding DTG curves are reported in Fig. 5. The data of FM and cRH are also reported for comparison. All the samples are stable up to 400°C and the carbonaceous part is completely burned off before 650°C. The burn-off of cRH_{NaOH} and cRH_{NaOH}-FM is anticipated, consistently with the higher porosity developed after the alkaline treatment compared to the parent materials (cRH). It is worth noticing that the burn-off temperature of cRH-FM is higher compared to that of both cRH and cRH_w. This result indicates that the magnetite shell shields the carbonaceous support from oxygen diffusion thus preventing the oxidation of the carbonaceous core. The amounts of final residue (i.e. the ashes) are consistent with those expected based on sorbent elemental analysis and ash content determination (Table 1). The highest residue is observed for cRH-FM.

3.2. Adsorption tests

Copper and lead ions adsorption isotherms for cRH, cRH_w, and cRH_{NaOH} are shown in Fig. 6. Copper and the lead ions adsorption isotherms for the two composites cRH-FM and cRH_{NaOH}-FM are reported in Figs. 7 and 8, respectively, along with those of bare FM and the parent carbonaceous support (cRH and cRH_{NaOH}, respectively). The plots are built up by reporting the adsorption capacity (q, mmol/g) as a function of the total metal concentration in solution at equilibrium conditions (c, mmol/L).

All the adsorption isotherms showed the typical L1 shape of the Giles classification [46], with an almost linear increase for very low concentrations and the tendency to approach a horizontal asymptote for high concentrations. It is well known that at low metal ion/adsorbent ratios, the adsorption process involves higher energy sites and a higher adsorption efficiency results while, as the metal ion/adsorbent ratio increases, being the higher energy sites saturated, the adsorption proceeds less efficiently involving lower energy active sites, often reaching an asymptotic, maximum adsorption capacity.

The experiments revealed that for larger concentrations, higher q values are detected in the case of copper ions adsorption tests, while at low concentrations, lead adsorption looks more effective. However, it is worth mentioning that when the adsorption capacity q is calculated as mg/g, higher q values are detected for lead adsorption in all the cases. Moreover, in the case of Pb adsorption isotherms on cRH, cRH_{NaOH}, and cRH_{NaOH}-FM, the approach to the horizontal asymptote is far from being reached, suggesting that the saturation of the adsorption sites is not achieved at the investigated range of metal ion initial concentrations (0 – 50 mg/L).

The chemical treatments performed on cRH lead to different effects on its adsorption properties. Simple washing with distilled water reduces the adsorption capacities of both copper and lead ions. When the cRH was treated with a strong alkaline solution (desilication), the corresponding adsorbent (cRH_{NaOH}) exhibited adsorption properties towards lead ions comparable to those of cRH, while a lower affinity towards copper ions (like that observed for distilled water washing) was found. The isotherms of the two composite materials show that the adsorption capacity of cRH_{NaOH}-FM is higher than that of the bare support (cRH_{NaOH}) for both copper and lead ions. The opposite result is shown for the adsorption capacities of cRH-FM, which are lower compared to those of cRH. In the case of cRH_{NaOH}-FM, a synergism between the carbonaceous support with a quite high surface area and the magnetite particles is suggested.

Looking at all the isotherms under equilibrium conditions, to correlate the adsorption performance with the textural properties of the materials, it is worth noting that the adsorption of lead ions seems to be more influenced by the surface area of the adsorbent than the adsorption of copper ions. In fact, the adsorption of lead ions increases as the surface area of the material increases. In the case of copper ions adsorption, this correlation does not hold, suggesting a predominant role for surface chemistry.

The adsorption of heavy metal ions on solid sorbents depends also on the solution pH since it influences the metal ion solubility and speciation, the chemical nature of the functional groups on the sorbent surface (ionization degree), and the counter ion concentration [47,48]. To investigate the effects of solution pH on the adsorption properties, the materials were exposed at 20 °C to solutions containing 10 mg/L of the metal ions at different initial pH values, below 6. These pH values have been selected for two main reasons: to limit the precipitation of metal hydroxides [29] and to test the adsorbents in conditions next to those of natural waters and wastewaters (most of the heavy metal-containing wastewaters are acidic). The corresponding adsorption isotherms at different equilibrium pH values are reported in Figs. 9 and 10 for copper and lead ions, respectively.

The results showed that the adsorption of lead and copper ions increases with the increase of solution pH, namely the sorption process is pH-dependent, as expected. The equilibrium pH depends on the sorbent and the metal ions hydrolysis. For the sorbents here considered, the pH established in water as a consequence of the hydrolysis of the sorbent functional groups [49] is between 6 and 7. In the working conditions, the solution pH was altered by the adsorption process, having variation above 1.5 pH units, especially for the samples at an initial pH of around 4. At low pH, the surface is protonated and the attraction towards metallic cations decreases due to electrostatic repulsion. At higher pH, the functional groups on the adsorbent surface become negatively charged and the electrostatic attraction between the adsorbent surface and cations increases [48,50,51]. The experiments show that, especially for low concentrations, the adsorption capacity scarcely depends on the pH value in the range between 4 and 7, while larger differences arise for pH values below 4. This result agrees with the findings of Zhang et al., 2011 [52] regarding the adsorption of copper ions by carbons produced by the physical activation of rice husk.

The adsorption of both metals between pH 4 and 6 is optimal, while a lower adsorption has been found in the case of solutions at pH 2, the latter interpreted by taking into account the complexation between metal ions and H_3O^+ ions. However, at pH higher than 7 in these model solutions, copper and lead hydroxides and hydroxide anions are formed, leading to a progressive reduction of the electrostatic attraction. It is worth mentioning that under basic pH conditions, the overall removal of copper and lead ions may be larger, thanks to the parallel precipitation, and microprecipitation (i.e. the formation of metal hydroxides precipitates over the sorbent surface), but it is no longer possible to distinguish between precipitation and adsorption, so that the reconstruction of the adsorption isotherm is no longer possible.

3.3. Data modelling and comparison with literature data

The adsorption data were analyzed considering the proposed additive-competitive Langmuir model [38–41] and the calculated parameters are listed in Table 3.

The R^2 values were above 0.96 in the case of Cu^{2+} adsorption data and above 0.87 in the case of Pb^{2+} adsorption data, indicating good accordance between experimental and simulated data and confirming the suitability of the proposed model to analyze the adsorption data. The good accordance between experimental and simulated data was also highlighted by the parity plots reported in Fig. 11 for Cu^{2+} and Pb^{2+} adsorption data.

Table 3 perfectly mirrors the features of the adsorption process observed in the experimental results in Figs. 6–8. The maximum adsorption capacity is larger for copper ions than for lead ions, but the energy of interaction for lead ions is much higher than that for copper ions. Besides, it is also worth noticing that the best fitting of data also indicates stronger effects of the solution pH on the adsorption of lead ions (this is mirrored by the higher values of K_H) either suggesting that the adsorption of copper and lead ions takes place on different sites or that the substitution of a H^+ ions with a Pb^{2+} ion on the active sites require more energy than that with a Cu^{2+} ion.

It is worth noting that the q_{max} values of cRH_{NaOH}-FM are higher than those of the corresponding bare support (cRH_{NaOH}) confirming the instauration of a synergistic effect between the carbonaceous support and the FM particles. This circumstance probably arises from an optimal dispersion of the FM phase on the support, as previously shown in the case of FM-based hybrid sorbents for CO_2 capture [34].

The calculated q_{max} values are compared with the theoretical adsorption capacity of rice husk-derived carbons reported by recent literature (Table 4). To simplify the comparison with most existing data, the adsorption capacities are reported in mg/g.

A great variability in q_{max} values is found and this is due to a range of factors that may affect q_{max} values of rice husk-derived carbons, mainly adsorbent production conditions (temperature, presence or absence of protection gas, heating rate, and pyrolysis/carbonization plant).

On the overall, the comparison with the literature confirms the higher affinity towards lead ions as found for the materials tested in this work. The Pb^{2+} q_{max} values calculated for the materials analyzed in this work are comparable and, in some cases, higher than those reported in the literature for bare biochar or ash from rice husk, while those related to Cu^{2+} adsorption are always lower. The Pb^{2+} q_{max} calculated for the two magnetic sorbents tested in this work is comparable to that of the magnetic material produced by Sun et al. [26] without $KMnO_4$ treatment (Table 4).

Finally, the partition factors H, m^3/kg, at low ion concentrations for the different operating conditions are shown in Table 5.

The experimental results indicated that the sole rice husk (cRH) is more selective toward lead than copper, but the NaOH-treated one (cRH_{NaOH}) and the rice husk–magnetite composites (cRH-FM and cRH_{NaOH}-FM) usually exploited higher partition coefficients.

3.4. Desorption tests

Preliminary desorption tests have been carried out on cRH and cRH_{NaOH}-FM using 1 M nitric acid. The experimental tests revealed that only a partial recovery of the captured metal ions can be taken from the sorbent, indicating the presence of multiple adsorption sites, some of which, around 40 %, exploit reversible adsorption while the remaining part shows a non-reversible adsorption. The fractions of reversible and non-reversible sites appear related to the physical-chemical characteristics of the parent RH, being similar for both cRH and cRH_{NaOH}-FM. The cyclic use of the sorbent, for three complete cycles, revealed that the number of active sites that can be desorbed at the first cycle is similar to that obtained at the third cycle. Much interestingly, elemental analysis and FTIR analysis on fresh and exhaust materials (after three adsorption/desorption cycles) do not reveal relevant alteration of the sorbent qualities (supporting information section, Table S3 and Figure S1, respectively). The desorption tests indicate a strong bonding of the metal ions with the surface functional groups and suggest further investigations involving the use of higher temperatures and more aggressive methods to allow cyclic use of the rice husk.

4. Conclusions

A set of composite materials has been prepared by coating carbonized rice husk (cRH) and its derivatives with iron oxide particles (FM). The obtained materials, containing an amount of FM between 5 and 10 wt%, were structurally characterized, and their adsorption performances toward Cu^{2+} and Pb^{2+} have been evaluated.

In all the cases an increase in the adsorption capacity is detected with the increase of the target metal ion concentration. The adsorption of both metals between pH 4 and 6 is optimal, while a lower absorption has been found in the case of solutions at pH 2. On the overall, a higher affinity towards lead ions was detected, in line with previous literature results on similar materials. The chemical treatments lead to different changes in the adsorption properties of cRH: simple washing with distilled water reduces the adsorption capacities towards both copper

and lead ions, and after desilication, the corresponding adsorbent (cRH_{NaOH}) exhibits adsorption properties towards lead ions comparable to those of cRH and a lower affinity towards copper ions. As concerns the composite materials, the adsorption capacity of cRH_{NaOH}-FM is higher than that of the bare support (cRH_{NaOH}) for both copper and lead ions. The opposite result is found for cRH-FM, which exhibits a lower affinity for both copper and lead ions compared to those of cRH. In the case of cRH_{NaOH}-FM, a synergism between the carbonaceous support with a quite high surface area and the magnetite particles is suggested.

For all the materials tested, the maximum adsorption capacity evaluated as mmol/g is larger for copper ions than for lead ions, but the energy of interaction for lead ions is much higher than that for copper ions. Besides, higher values of K_H were calculated by modeling the experimental data by the additive-competitive Langmuir model, suggesting that the adsorption of copper and lead ions takes place on different sites or that the substitution of H_3O^+ ions with a Pb^{2+} ion on the active sites requires more energy than that with the Cu^{2+}. Besides, the experiments suggested that cRH-FM composites are more selective toward copper than lead ions at low concentrations, where higher partition factors have been observed. Finally, preliminary desorption tests indicated that further efforts are needed to provide complete reversibility of copper and lead ions adsorption, being the presence of reversible and non-reversible adsorption sites derived from the structure of the parent cRH rather than from the formulation of the cRH-FM composites.

CRediT authorship contribution statement

Michela Alfe: Writing – review & editing, Validation, Supervision, Resources, Project administration, Methodology, Funding acquisition, Conceptualization. **Valentina Gargiulo:** Writing – review & editing, Writing – original draft, Visualization, Validation, Methodology, Investigation, Data curation, Conceptualization. **Francesco Di Natale:** Writing – review & editing, Validation, Resources, Methodology, Funding acquisition, Formal analysis, Conceptualization.

Declaration of Competing Interest

The authors declare that they have no known competing financial interests or personal relationships that could have appeared to influence the work reported in this paper.

Data Availability

Data will be made available on request.

Acknowledgments

The assistance of P. Giudicianni (BET), L. Cortese (SEM-EDX), L. Stanzione and A. Capuozzo (XRF analysis) and F. Stanzione (ICP-MS) from CNR-STEMS was kindly acknowledged. VG and MA acknowledge the networking support by the COST (European Cooperation in Science and Technology) Action CA20127 WIRE.

Appendix A. Supporting information

Supplementary data associated with this article can be found in the online version at doi:10.1016/j.jece.2024.113497.

References

[1] Q. Zhou, N. Yang, Y. Li, B. Ren, X. Ding, H. Bian, X. Yao, Total concentrations and sources of heavy metal pollution in global river and lake water bodies from 1972 to 2017, Glob. Ecol. Conserv. 22 (2020) e00925, https://doi.org/10.1016/j.gecco.2020.e00925.

[2] K.H.H. Aziz, F.S. Mustafa, K.M. Omer, S. Hama, R.F. Hamarawf, K.O. Rahman, Heavy metal pollution in the aquatic environment: efficient and low-cost removal approaches to eliminate their toxicity: a review, RSC Adv. 13 (2023) 17595, https://doi.org/10.1039/D3RA00723E.

[3] J. Briffa, E. Sinagra, R. Blundell, Heavy metal pollution in the environment and their toxicological effects on humans, Heliyon 6 (2020) e04691, https://doi.org/10.1016/j.heliyon.2020.e04691.

[4] M. Ahmaruzzaman, V.K. Gupta, Rice husk and its ash as low-cost adsorbents in water and wastewater treatment, Ind. Eng. Chem. Res. 50 (2011) 13589–13613, https://doi.org/10.1021/ie201477c.

[5] S. Sobhanardakani, H. Parvizimosaed, E. Olyaie, Heavy metals removal from wastewaters using organic solid waste—rice husk, Environ. Sci. Pollut. Res 20 (2013) 5265–5271, https://doi.org/10.1007/s11356-013-1516-1.

[6] A. Bhatnagar, M. Sillanpää, Utilization of agro-industrial and municipal waste materials as potential adsorbents for water treatment—a review, Chem. Eng. J. 157 (2010) 277–296, https://doi.org/10.1016/j.cej.2010.01.007.

[7] A.T. Hoang, S. Kumar, E. Lichtfouse, C.K. Cheng, R.S. Varma, N. Senthilkumar, P.Q. P. Nguyen, X.P. Nguyen, Remediation of heavy metal polluted waters using activated carbon from lignocellulosic biomass: an update of recent trends, Chemosphere 302 (2022) 134825, https://doi.org/10.1016/j.chemosphere.2022.134825.

[8] M. Lewoyehu, Comprehensive review on synthesis and application of activated carbon from agricultural residues for the remediation of venomous pollutants in wastewater, J. Anal. Appl. Pyrolysis 159 (2021) 105279, https://doi.org/10.1016/j.jaap.2021.105279.

[9] V. Gargiulo, M. Alfè, P. Ammendola, F. Raganati, R. Chirone, CO2 sorption on surface-modified carbonaceous support: probing the influence of the carbon black microporosity and surface polarity, Appl. Surf. Sci. 360 (Part A) (2016) 329–337, https://doi.org/10.1016/j.apsusc.2015.11.026.

[10] V.V. Krishna, M. Mkondiwa, Economics of crop residue management, Annu. Rev. Resour. Econ. 15 (2023) 19–39, https://doi.org/10.1146/annurev-resource-101422-090019.

[11] H.A. Hegazi, Removal of heavy metals from wastewater using agricultural and industrial wastes as adsorbents Housing and Building National Research Center, HBRC J. 9 (2013) 276–282, https://doi.org/10.1016/j.hbrcj.2013.08.004.

[12] T.A.H. Nguyen, H.H. Ngo, W.S. Guo, J. Zhang, S. Liang, Q.Y. Yue, Q. Li, T. V. Nguyen, Applicability of agricultural waste and by-products for adsorptive removal of heavy metals from wastewater, Bioresour. Technol. 148 (2013) 574–585, https://doi.org/10.1016/j.biortech.2013.08.124.

[13] J.U. Ani, K.G. Akpomie, U.C. Okoro, L.E. Aneke, O.D. Onukwuli, O.T. Ujam, Potentials of activated carbon produced from biomass materials for sequestration of dyes, heavy metals, and crude oil components from aqueous environment, Appl. Water Sci. 10 (2020) 69, https://doi.org/10.1007/s13201-020-1149-8.

[14] D.S. Karam, P. Nagabovanalli, K.S. Rajoo, C.F. Ishak, A. Abdu, Z. Rosli, F. M. Muharam, D. Zulperi, An overview on the preparation of rice husk biochar, factors affecting its properties, and its agriculture application, J. Saudi Soc. Agric. Sci. 21 (3) (2022) 149–159, https://doi.org/10.1016/j.jssas.2021.07.005.

[15] Z. Shamsollahi, A. Partovinia, Recent advances on pollutants removal by rice husk as a bio-based adsorbent: A critical review, J. Environ. Manag. 246 (2019) 314–323, https://doi.org/10.1016/j.jenvman.2019.05.145.

[16] H.K. Okoro, S.M. Alao, S. Pandey, I. Jimoh, K.A. Basheeru, Z. Caliphs, J.C. Ngila, Recent potential application of rice husk as an eco-friendly adsorbent for removal of heavy metals, Appl. Water Sci. 12 (2022) 259, https://doi.org/10.1007/s13201-022-01778-1.

[17] N. Soltani, A. Bahrami, M.I. Pech-Canul, L.A. González, Review on the physicochemical treatments of rice husk for production of advanced materials, Chem. Eng. J. 264 (2015) 899–935, https://doi.org/10.1016/j.cej.2014.11.056.

[18] S.S. Shukla, R. Chava, S. Appari, B. A, B.V.R. Kuncharam, Sustainable use of rice husk for the cleaner production of value-added products, J. Environ. Chem. Eng. 10 (2022) 106899, https://doi.org/10.1016/j.jece.2021.106899.

[19] B. Bushra, N. Remya, Biochar from pyrolysis of rice husk biomass—characteristics, modification and environmental application, Biomass-.-. Convers. Biorefin. (2020) 1–12, https://doi.org/10.1007/s13399-020-01092-3.

[20] N.T. Luyen, H.X. Linh, T.Q. Huy, Preparation of rice husk biochar-based magnetic nanocomposite for effective removal of crystal violet, J. Electron. Mater. 49 (2) (2020) 1142–1149, https://doi.org/10.1007/s11664-019-07798-z.

[21] W. Guo, S. Wang, Y. Wang, S. Lu, Y. Gao, Sorptive removal of phenanthrene from aqueous solutions using magnetic and non-magnetic rice husk-derived biochars, R. Soc. Open Sci. 5 (2018) 172382, https://doi.org/10.1098/rsos.172382.

[22] C.P. Lawagon, R.E.C. Amon, Magnetic rice husk ash 'cleanser' as efficient methylene blue adsorbent, Environ. Eng. Res. 25 (5) (2020) 685–692, https://doi.org/10.4491/eer.2019.287.

[23] J. Lou, X. Xu, Y. Gao, D. Zheng, J. Wang, Z. Li, Preparation of magnetic activated carbon from waste rice husk for the determination of tetracycline antibiotics in water samples, RSC Adv. 6 (2016) 112166, https://doi.org/10.1039/C6RA24397E.

[24] P. Li, S. Wang, B. Lv, M. Zhang, C. Xing, X. Sun, Y. Fang, Magnetic rice husk-based biochar for removal of aflatoxin B1 from peanut oil, Food Control 152 (2023) 109883, https://doi.org/10.1016/j.foodcont.2023.109883.

[25] K. Javed, S. Mahmood, M. Ammar, N. Abbas, M.Y. Shah, T. Ahmed, G. Mustafa, Rice husk ash adsorbent modified by iron oxide with excellent adsorption capacity for arsenic removal from water, Int. J. Environ. Sci. Technol. 20 (2023) 2819–2828, https://doi.org/10.1007/s13762-022-04390-7.

[26] C. Sun, T. Chen, Q. Huang, J. Wang, S. Lu, J. Yan, Enhanced adsorption for Pb(II) and Cd(II) of magnetic rice husk biochar by KMnO4 modification, Environ. Sci. Pollut. Res. 26 (2019) 8902–8913, https://doi.org/10.1007/s11356-019-04321-z.

[27] S. Zhang, S. Zhu, H. Zhang, X. Liu, Y. Xiong, Synthesis and characterization of rice husk-based magnetic porous carbon by pyrolysis of pretreated rice husk with $FeCl_3$

and $ZnCl_2$, J. Anal. Appl. Pyrolysis 147 (2020) 104806, https://doi.org/10.1016/j.jaap.2020.104806.
[28] L.R. Marcelo, J. Santos de Gois, A. Araujo da Silva, D. Vargas Cesar, Synthesis of iron-based magnetic nanocomposites and applications in adsorption processes for water treatment: a review (oi.org/), Environ. Chem. Lett. 19 (2021) 1229–1274, https://doi.org/10.1007/s10311-020-01134-2.
[29] M. Benjamin, Water chemistry, McGraw Hill, 2002.
[30] W. Stumm, J.J. Morgan. Aquatic Chemistry, Chemical Equilibria and Rates in Natural Waters, 3rd Edition, John Wiley & Sons, Inc, New York, 1996.
[31] G. Hotová, V. Slovák, T. Zelenka, R. Maršálek, A. Parchaňská, The role of the oxygen functional groups in adsorption of copper (II) on carbon surface, Sci. Total Environ. 711 (2020) 135436, https://doi.org/10.1016/j.scitotenv.2019.135436.
[32] P. Zhao, Z. Huang, P. Wang, A. Wang, Comparative study on high-efficiency Pb(II) removal from aqueous solutions using coal and rice husk based humic acids, J. Mol. Liq. 369 (2023) 120875, https://doi.org/10.1016/j.molliq.2022.120875.
[33] V. Gargiulo, M. Alfè, F. Raganati, A. Zhumagaliyeva, Y. Doszhanov, P. Ammendola, R. Chirone, CO_2 Adsorption under Dynamic Conditions: An Overview on Rice Husk-Derived Sorbents and Other Materials, Combust. Sci. Technol. 191 (9) (2019) 1484–1498, https://doi.org/10.1080/00102202.2018.1546697.
[34] M. Alfè, P. Ammendola, Valentina Gargiulo, F. Raganati, R. Chirone, Magnetite loaded carbon fine particles as low-cost CO2 adsorbent in a sound assisted fluidized bed, Proc. Combust. Inst. 35 (2015) 2801–2809.
[35] M. Thommes, K. Kaneko, A.V. Neimark, J.P. Olivier, F. Rodriguez-Reinoso, J. Rouquerol, K.S.W. Sing, Physisorption of gases, with special reference to the evaluation of surface area and pore size distribution (IUPAC Technical Report), Pure Appl. Chem. 87 (2015) 1051–1069, https://doi.org/10.1515/pac-2014-1117.
[36] J. Rouquerol, F. Rouquerol, P. Llewellyn, G. Maurin, K. Sing, Adsorption by powders and porous solids: principles, methodology and applications, Academic Press, 2013.
[37] F. Di Natale, V. Gargiulo, M. Alfè, Adsorption of heavy metals on silica-supported hydrophilic carbonaceous nanoparticles (SHNPs), J. Hazard. Mater. 393 (2020) 122374, https://doi.org/10.1016/j.jhazmat.2020.122374.
[38] F. Di Natale, A. Erto, A. Lancia, D. Musmarra, Mercury adsorption on granular activated carbon in aqueous solutions containing nitrates and chlorides, J. Hazard. Mater. 192 (3) (2011) 1842–1850, https://doi.org/10.1016/j.jhazmat.2011.07.021.
[39] A. Erto, F. Di Natale, D. Musmarra, A. Lancia, Modeling of single and competitive adsorption of cadmium and zinc onto activated carbon, Adsorption 21 (8) (2015) 611–621, https://doi.org/10.1007/s10450-015-9712-6.
[40] F. Di Natale, A. Erto, A. Lancia, D. Musmarra, Equilibrium and dynamic study on hexavalent chromium adsorption onto activated carbon, J. Hazard. Mater. 281 (8) () (2015) 47–55, https://doi.org/10.1016/j.jhazmat.2014.07.072.
[41] F. Di Natale, A. Erto, A. Lancia, D. Musmarra, A descriptive model for metallic ions adsorption from aqueous solutions onto activated carbons, J. Hazard. Mater. 169 (1-3) (2009) 360–369, https://doi.org/10.1016/j.jhazmat.2009.03.105.
[42] C. Miranda, V.K. Booth, M.R. Morrow, Effects of amphipathic polypeptides on membrane organization inferred from studies using bicellar lipid mixtures, Langmuir 34 (39) (2018) 11759–11771, https://doi.org/10.1021/acs.langmuir.8b02257.
[43] A. Basu, S.S. Ali, S.S. Hossain, M. Asif, A Review of the Dynamic Mathematical Modeling of Heavy Metal Removal with the Biosorption Process, Processes 10 (2022) 1154, https://doi.org/10.3390/pr10061154.
[44] J.G. Amrutha, C.R. Girish, B. Prabhu, K. Mayer, Multi-component adsorption isotherms: review and modeling studies, Environ. Process. 10 (2) (2023) 38, https://doi.org/10.1007/s40710-023-00631-0.
[45] M.E. Compeán-Jasso, F. Ruiz, J.R. Martínez, A. Herrera-Gómez, Magnetic properties of magnetite nanoparticles synthesized by forced hydrolysis, Mater. Lett. 62 (27) (2008) 4248–4250, https://doi.org/10.1016/j.matlet.2008.06.053.
[46] C.H. Giles, D. Smith, A. Huitson, A general treatment and classification of the solute adsorption isotherm. J. Colloid Interface Sci. 47 (3) (1974) 755–765, https://doi.org/10.1016/0021-9797(74)90252-5.
[47] E. Asrari, H. Tavallali, M. Hagshenas M, Removal of Zn(II) and Pb (II) ions using rice husk in food industrial wastewater, J. Appl. Sci. Environ. Manag. 14 (2010) 159–162, https://doi.org/10.4314/jasem.v14i4.63306.
[48] M. Masih, P. Anthony, S.H. Siddiqui, Removal of Cu (II) ion from aqueous solutions by Rice Husk Carbon-Chitosan Composite gel (CCRH) using response surface methodology, Environ. Nanotechnol. Monit. Manag. 10 (2018) 189–198, https://doi.org/10.1016/j.enmm.2018.07.003.
[49] J.S. Noh, J.A. Schwarz, Effect of HNO3 treatment on the surface acidity of activated carbons, Carbon 28 (1990) 675–682, https://doi.org/10.1016/0008-6223(90)90069-B.
[50] P.L. Homagai, K.N. Ghimire, K. Inoue, Adsorption behavior of heavy metals onto chemically modified sugarcane bagasse, Bioresour. Technol. 101 (6) (2010) 2067–2069, https://doi.org/10.1016/j.biortech.2009.11.073.
[51] R. Mallampati, S. Valiyaveettil, Application of tomato peel as an efficient adsorbent for water purification—alternative biotechnology? RSC Adv. 2 (2012) 9914–9920, https://doi.org/10.1039/C2RA21108D.
[52] J. Zhang, H. Fu, X. Lv, J. Tang, X. Xu, Removal of Cu(II) from aqueous solution using the rice husk carbons prepared by the physical activation process, Biomass-.-. Bioenergy 35 (2011) 464–472, https://doi.org/10.1016/j.biombioe.2010.09.002.
[53] M.F. Taha, A.S. Shuib, M.S. Shaharun, A. Borhan, Removal of Ni(II), Zn(II) and Pb (II) ions from single metal aqueous solution using rice husk-based activated carbon, AIP Conf. Proc. 1621 (2014) 210, https://doi.org/10.1063/1.4898468.
[54] R.I. Babatunde, A.A. Ibrahim, Removal of heavy metal from waste water using activated carbon from rice husk, Int. J. Adv. Sci. Res. Eng. 6 (2020) 104–112, https://doi.org/10.31695/IJASRE.2020.33724.
[55] J. Shi, X. Fan, D.C.W. Tsang, F. Wang, Z. Shen, D. Hou, D.S. Alessi, Removal of lead by rice husk biochars produced at different temperatures and implications for their environmental utilizations, Chemosphere 235 (2019) 825–831, https://doi.org/10.1016/j.chemosphere.2019.06.237.
[56] T.K. Naiya, A.K. Bhattacharya, S. Mandal, S.K. Das, The sorption of lead(II) ions on rice husk ash, J. Hazard. Mater. 163 (2009) 1254–1264, https://doi.org/10.1016/j.jhazmat.2008.07.119.
[57] P. Vassileva, A. Detcheva, I. Uzunov, S. Uzunova, Removal of metal ions from aqueous solutions using pyrolyzed rice husks: adsorption kinetics and equilibria, Chem. Eng. Commun. 200 (12) (2013) 1578–1599, https://doi.org/10.1080/00986445.2012.755519.
[58] X. Xu, X. Cao, L. Zhao, Comparison of rice husk- and dairy manure-derived biochars for simultaneously removing heavy metals from aqueous solutions: Role of mineral components in biochars, Chemosphere 92 (2013) 955–961, https://doi.org/10.1016/j.chemosphere.2013.03.009.
[59] K. Aswini, V. Jaisankar, Adsorption treatment of heavy metal removal from simulated waste water using rice husk activated carbon (Rhac) and its polyvinylpyrrolidone (PVP) composite as an adsorbent, J. Water Environ. Sci. 3 (1) (2019) 460–470.
[60] P.M. Sanka, M.J. Rwiza, K.M. Mtei, Removal of selected heavy metal ions from industrial wastewater using rice and corn husk biochar, Water Air Soil Pollut. 231 (2020) 244, https://doi.org/10.1007/s11270-020-04624-9.
[61] B. Roha, J. Yao, A. Batool, R. Hameed, M.A. Ghufran, M.T. Hayat, G. Sunahara, Model sorption of industrial wastewater containing Cu2+, Cd2+, and Pb2+ using individual and mixed rice husk biochar, Environ. Technol. Innov. 24 (2021) 101900, https://doi.org/10.1016/j.eti.2021.101900.
[62] U. Kamran, S.-Y. Lee, K.Y. Rhee, S.-J. Park, Rice husk valorization into sustainable Ni@TiO2/biochar nanocomposite for highly selective Pb (II) ions removal from an aqueous media, Chemosphere 323 (2023) 138210, https://doi.org/10.1016/j.chemosphere.2023.138210.
[63] P. Wijeyawardana, N. Nanayakkara, C. Gunasekara, A. Karunarathna, D. Law, B. K. Pramanik, Removal of Cu, Pb and Zn from stormwater using an industrially manufactured sawdust and paddy husk derived biochar, Environ. Technol. Innov. 28 (2022) 102640, https://doi.org/10.1016/j.eti.2022.102640.
[64] X. Zhang, Z. Gao, X. Fan, L. Tan, Y. Jiang, W. Zheng, F.X. Han, Y. Liang, A comparative study on adsorption of cadmium and lead by hydrochars and biochars derived from rice husk and Zizania latifolia straw, Environ. Sci. Pollut. Res. 29 (2022) 63768–63781, https://doi.org/10.1007/s11356-022-20263-5.
[65] C. Gai, Y. Guo, N. Peng, T. Liu, Z. Liu, N-Doped biochar derived from co-hydrothermal carbonization of rice husk and Chlorella pyrenoidosa for enhancing copper ion adsorption, RSC Adv. 6 (2016) 53713.